![Nano Research logo]

Bioinspired supramolecular macrocycle hybrid membranes with enhanced proton conductivity

Pengfei Yang[§], Linlin Xu[§], Panagiotis Trogadas, Marc-Olivier Coppens, and Yang Lan (✉)

Centre for Nature Inspired Engineering, Department of Chemical Engineering, University College London, London WC1E 7JE, UK
[§] *Pengfei Yang and Linlin Xu contributed equally to this work.*

ABSTRACT

Enhancing the proton conductivity of proton exchange membranes (PEMs) is essential to expand the applications of proton exchange membrane fuel cells (PEMFCs). Inspired by the proton conduction mechanism of bacteriorhodopsin, cucurbit[n]urils (CB[n], where n is the number of glycoluril units, n = 6, 7, or 8) are introduced into sulfonated poly(ether ether ketone) (SPEEK) matrix to fabricate hybrid PEMs, employing a nature-inspired chemical engineering (NICE) methodology. The carbonyl groups of CB[n] act as proton-conducting sites, while the host–guest interaction between CB[n] and water molecules offers extra proton-conducting pathways. Additionally, the molecular size of CB[n] aids in their dispersion within the SPEEK matrix, effectively bridging the unconnected proton-conducting sulfonic group domains within the SPEEK membrane. Consequently, all hybrid membranes exhibit significantly enhanced proton conductivity. Notably, the SPEEK membrane incorporating 1 wt.% CB[8] (CB[8]/SPEEK-1%) demonstrates the highest proton conductivity of 198.0 mS·cm^{-1} at 60 °C and 100% relative humidity (RH), which is 228% greater than that of the pure SPEEK membrane under the same conditions. Moreover, hybrid membranes exhibit superior fuel cell performance. The CB[8]/SPEEK-1% membrane achieves a maximum power density of 214 mW·cm^{-2}, representing a 140% improvement over the pure SPEEK membrane (89 mW·cm^{-2}) at 50 °C and 100% RH. These findings serve as a foundation for constructing continuous proton-conducting pathways within membranes by utilizing supramolecular macrocycles as fuel cell electrolytes and in other applications.

KEYWORDS

supramolecular macrocycle, proton conductivity, cucurbit[n]uril, proton exchange membrane, fuel cell

1 Introduction

Proton exchange membrane fuel cells (PEMFCs) have emerged as a compelling solution in the energy transition, thanks to their remarkable energy conversion efficiency and environmental sustainability, particularly when powered by green hydrogen [1]. Proton exchange membranes (PEMs) are the key component of PEMFCs, which segregate the anode and cathode and enable rapid and selective proton transport [2, 3]. Nowadays, the widely adopted PEM is a perfluorinated sulfonic acid membrane, such as Nafion® produced by Dupont, which exhibits excellent proton conductivity and fuel cell performance [4]. However, Nafion has certain drawbacks, notably its high cost [5]. Consequently, considerable efforts have been devoted to developing alternative PEMs such as sulfonated poly(ether ether ketone) (SPEEK) and sulfonated poly(ether sulfone) (SPES), renowned for their cost-effectiveness as well as their elevated thermal and mechanical stability [6]. Nonetheless, the proton conductivity of these alternative PEMs suffers from lower proton conductivity due to the smaller sulfonic acid aggregates within SPEEKs and SPESs, which results in fewer interconnected proton-conducting domains compared with Nafion [7, 8].

In recent decades, incorporating fillers into the polymer matrix has emerged as a successful approach to enhance proton conductivity by establishing more efficient proton-conducting pathways [9]. Various fillers, including nanofibers [10], nanotubes [11], graphene oxide [12], metal-organic frameworks [13], and covalent-organic frameworks [14], have exhibited proton-conducting capabilities because of their well-defined proton-binding sites. By introducing these fillers, hybrid membranes benefit from additional proton-conducting sites and structured pathways, thereby facilitating proton conduction within the membranes [15–18]. However, the poor compatibility between the filler and the polymer matrix always results in aggregation of fillers within the membrane, which causes flaws and dead zones in the membrane, consequently leading to reduced proton conductivity [19–22]. Hence, the selection of an ideal filler material becomes pivotal in the advancement of PEMs.

Bacteriorhodopsin, a membrane protein, which transports protons across the cell membrane of the halophilic organism *Halobacterium salinarum* [23], serves as a natural inspiration for PEMs. Bacteriorhodopsin harvests the light energy to drive conformational changes that facilitate unidirectional proton transport across the cell membrane [24]. This process involves the transport of protons through a hydrophobic cavity, reducing the proton affinity and minimizing the energy barrier associated with proton conduction. Concurrently, hydrogen bond interactions occur, involving the breaking and recombination of bonds

between water molecules, proton donors, and acceptors [24]. In this work, we adopt a nature-inspired chemical engineering (NICE) methodology, developed over the last two decades to promote sustainable solutions to engineering challenges in areas including catalysis, fluidization, fuel cells, and membrane separations, to explore the potential of supramolecular macrocycles as filler candidates for PEMs by drawing from the proton transport features of bacteriorhodopsin ("nature", Scheme 1) [25–27]. Specifically, cucurbit[n]urils (CB[n], where n is the number of glycoluril units, n = 6, 7, or 8), a series of supramolecular macrocycles with hydrophobic cavity and remarkable proton conductivity (> 10 mS·cm⁻¹) [28, 29], are investigated as fillers in SPEEK matrix for PEMs for the first time, based on the best of our knowledge. The cavity of CB[n] allows for hosting guest molecules such as water and acid molecules, facilitating proton transfer through host–guest interaction [30, 31]. Protons can swiftly navigate along the hydrogen bond networks formed by the carbonyl groups of CB[n] and guest molecules via the Grotthuss mechanism and the vehicle mechanism ("nature-inspired concept", Scheme 1) [32, 33]. In addition, CB[n] molecules are of molecular scale (< 2 nm) and possess organic molecular structures that align well with the polymer matrix of membrane, ensuring their proper dispersion without causing voids or dead zones ("nature-inspired design", Scheme 1) [10, 34, 35]. CB[n] (n = 6, 7, or 8) are introduced separately into the SPEEK matrix by solution casting to fabricate hybrid membranes for PEMs ("prototype", Scheme 1). Consequently, the most suitable candidate CB[n] is selected based on the conductivity of PEMs, and their PEMFC performance is investigated with varying loading amount of CB[n] ("application", Scheme 1).

2 Experimental

2.1 Synthesis of SPEEK

Poly(ether ether ketone) (PEEK, 14.0 g, Polysciences Inc.) was pre-dried in a vacuum oven overnight at 80 °C. Dried PEEK pellets were slowly added into a vigorously mechanically stirred 100 mL sulfuric acid (98 wt.%, Merck & Co.) solution in a three-neck round-bottom flask at 50 °C for 10 h [36]. Then, the polymer solution was gradually precipitated into ice-cold water bath with mechanical stirring. The polymer suspension was placed to settle overnight. The polymer precipitate was filtered, washed several times with deionized (DI) water until pH was neutral, and then dried under vacuum at 60 °C for 24 h.

2.2 Preparation of CB[n]/SPEEK

CB[n] (n = 6, 7, or 8) were synthesized and purified as reported previously [37, 38]. As-prepared SPEEK was dissolved in dimethylformamide (DMF, Merck & Co.) with magnetic stirring to make an SPEEK solution with 5 wt.% concentration. A certain amount of CB[n] (n = 6, 7, or 8) was added to the SPEEK solution to form the CB[n]/SPEEK hybrid membrane, named as CB[n]/SPEEK-X%, where X is the weight percent of CB[n] to SPEEK. The mixture was dispersed by an ultrasonic homogenizer for 5 min. Then, the membrane solution was cast on a dry glass and kept in the oven at 60 °C for 24 h. The pure SPEEK membrane and the SPEEK membranes with different weight percents of CB[8] were prepared by the same method.

2.3 Characterization

The morphology of the membranes' cross-section was characterized by scanning electron microscopy (SEM). The chemical structure of membranes was characterized by attenuated total reflectance Fourier transform infrared (ATR-FTIR) spectroscopy.
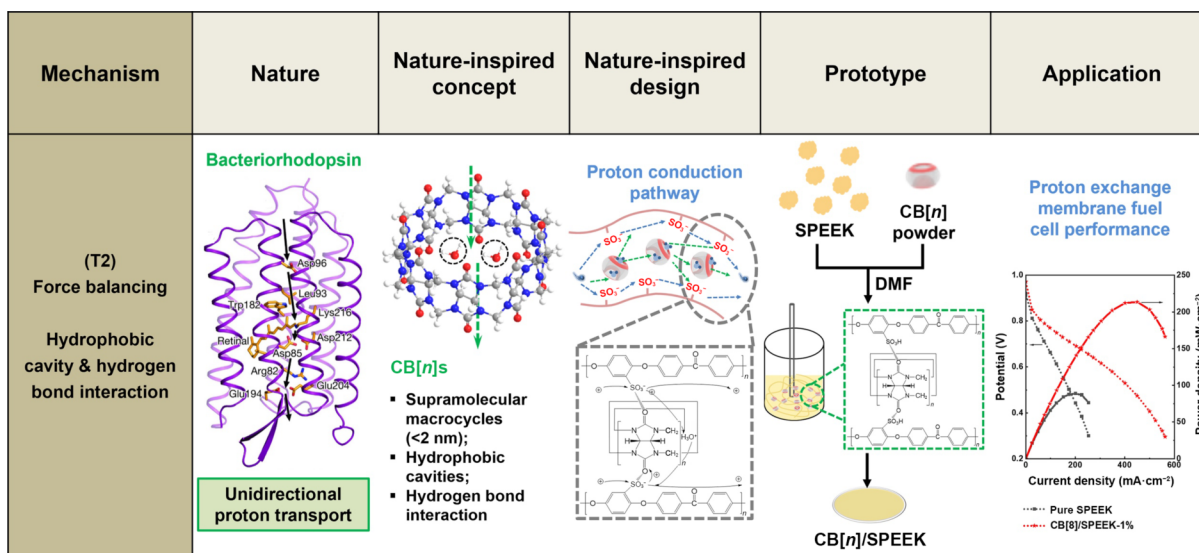
2.4 Proton conductivity

After drying the CB[n]/SPEEK hybrid membrane at 60 °C for 12 h, the proton conductivity (σ, mS·cm⁻¹) of all membranes was measured through two-electrode alternating current (AC) impedance spectroscopy at 100% relative humidity (RH) and calculated through Eq. (1) [36]

$$\sigma = \frac{l}{Sr} \tag{1}$$

where l (cm) is the length between two electrodes, S (cm²) is the cross-section area of the membrane sample, and r (kΩ) is the AC resistance of the membranes, respectively.

The activation energy (E_a, eV) of the proton conduction process was calculated through the Arrhenius equation as shown in Eq. (2) [39], which implied a linear relationship between T^{-1} and $\ln\sigma$

$$\ln\sigma = -\frac{E_a}{RT} + \ln\sigma_0 \tag{2}$$

| Mechanism | Nature | Nature-inspired concept | Nature-inspired design | Prototype | Application |

Scheme 1 Nature-inspired engineering of proton exchange membranes to realize effective proton transfer through CB[n], as in bacteriorhodopsin. Reproduced with permission from Ref. [24], © American Association for the Advancement of Science 2016.

where R is the ideal gas constant, T (K) is the absolute temperature, and $\ln\sigma_0$ is the y-intercept, respectively.

2.5 Water uptake and swelling degree of CB[n]/SPEEK

The CB[n]/SPEEK hybrid membranes were dried at 60 °C for 24 h until the weight became constant before water uptake and the swelling degree tests. Then, the weights and area of all membranes were measured immediately after being taken out from the oven. All membranes were kept in a 100% RH atmosphere for 24 h at 30 and 60 °C, respectively. The membranes were taken out and the weights and areas of all samples were measured immediately after the surface water was removed. The calculations of the water uptake and swelling degree of all samples were conducted through Eqs. (3) and (4), respectively [14]

$$\text{Water uptake} = \frac{W_{\text{wet}} - W_{\text{dry}}}{W_{\text{dry}}} \tag{3}$$

$$\text{Swelling degree} = \frac{A_{\text{wet}} - A_{\text{dry}}}{A_{\text{dry}}} \tag{4}$$

where W_{dry} (g) and W_{wet} (g) are the weights of the membranes before and after treatment, and A_{dry} (cm^2) and A_{wet} (cm^2) are their areas before and after treatment, respectively.

2.6 Ion exchange capacity (IEC) of CB[n]/SPEEK

CB[n]/SPEEK and SPEEK membranes were dried at 60 °C for 24 h until the weight became constant. The samples were immersed in NaCl solution (0.1 M) for 24 h without stirring. After 24 h, the membranes were removed from the solution, phenolphthalein was added into the solution as color change indicator, and the solution was titrated against 0.1 M NaOH ($M_{\text{NaOH}} = 0.1$ mol·L^{-1}) until a light pink colour appeared. Then, the ion exchange capacity (mmol·g^{-1}) could be obtained by: IEC = ($V_{\text{NaOH}} \times M_{\text{NaOH}}$)/$W_{\text{dry}}$, where V_{NaOH} (mL) represents the consumption volume of NaOH solution [14].

2.7 Fuel cell performance

The membrane electrode assembly (MEA) with active area of 4 cm^2 was prepared in-house by hot pressing of prepared membranes and HyPlat gas diffusion electrodes (HyPlat) using a thermal press (Carver Auto Series Plus) at 150 °C for 3 min under an applied mass of 1700 lb. The catalyst layers had a platinum loading of 0.4 mg$_{\text{Pt}}$·cm^{-2} at both the cathode and anode. The single fuel cell test was carried out using a Scribner 850e fuel cell test station (Scribner Associates). The stoichiometric ratios of the anode and cathode were kept constant at 1.5 and 3, respectively.

Inlet air and hydrogen were humidified using bubbler-type humidifier tanks. Each gas was fed through a bubbler at the bottom of the water tank, and dew points were regulated by controlling the temperature of the water. The inlet gas RH of the anode and cathode was kept the same at 100%, and the cell temperature was set to 50 °C. The outlet of both the anode and cathode was at atmospheric pressure. Polarization curves were obtained by taking data points between open-circuit voltage (OCV) and 0.3 V.

3 Results and discussion

3.1 Physical morphology of the membranes

The morphology analysis of the membranes was performed using SEM. The cross-sectional SEM images are shown in Fig. 1. The pure SPEEK membrane exhibits a compact and defect-free structure, as depicted in Fig. 1(a). Upon the incorporation of CB[n], the CB[n]/SPEEK membranes with 1 wt.% CB[n] ($n = 6, 7$, or 8) maintain the same desirable defect-free structure as the pure SPEEK membrane, as observed in Figs. 1(b)–1(d). Notably, the CB[n] fillers exhibit excellent dispersion within the SPEEK matrix, devoid of significant aggregates or voids. This favorable dispersion is attributed to the molecular-scale size of the CB[n] (< 2 nm) [40, 41] and the organic molecular structure of CB[n] ensuring the high compatibility with the SPEEK matrix [10, 34, 35]. Similarly, hybrid membranes with different amounts of CB[8] (CB[8]/SPEEK-X%, X = 0.2, 0.5, 1, and 2) also show defect-free structures, as shown in Figs. 1(d)–1(g).

3.2 Chemical structures of the membranes

The chemical composition of the membranes was examined using ATR-FTIR spectroscopy. As shown in Fig. 2(a), the spectra of all membranes show a clear peak band at 1646 cm^{-1}, which is ascribed to the vibration of C=O of SPEEK [42]. The characteristic peaks at 1249, 1079, and 1024 cm^{-1} are attributed to the vibration of O=S=O of the sulfonic groups on the SPEEK backbones [13]. After the addition of CB[6], CB[7], and CB[8], an inconspicuous peak shows at 1737 cm^{-1} in the spectra of the corresponding membranes, which corresponds to the characteristic peak of the C=O of CB[n] [43]. The position of the C=O peak of CB[n] is different from that of SPEEK, which is ascribed to the distinct chemical environments where C=O groups are located. The C=O groups of CB[n] reside at the ports and bond with the –N–H, while the C=O groups of SPEEK bond with the benzene rings [43]. Similar chemical profiles are also observed in the spectra of
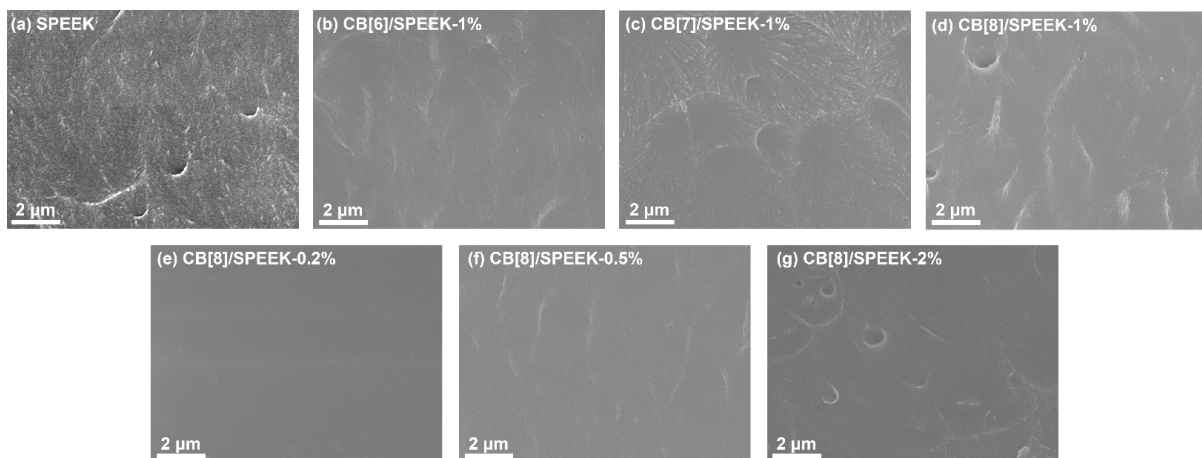
Figure 1 The cross-sectional SEM images of (a) pure SPEEK, (b) CB[6]/SPEEK-1%, (c) CB[7]/SPEEK-1%, (d) CB[8]/SPEEK-1%, (e) CB[8]/SPEEK-0.2%, (f) CB[8]/SPEEK-0.5%, and (g) CB[8]/SPEEK-2% membranes. Percentage means the weight percent of CB[n] to the SPEEK matrix.
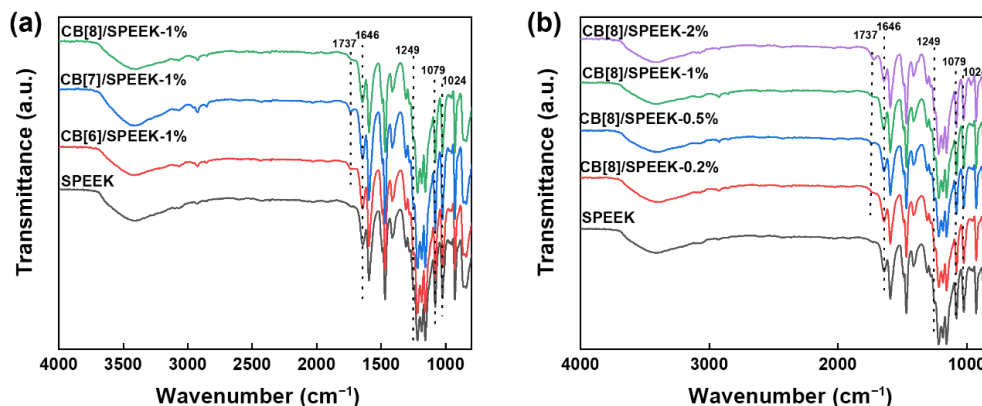
Figure 2 ATR-FTIR spectra for different membranes: (a) SPEEK membranes with 1 wt.% CB[*n*], *n* = 6, 7, or 8, and (b) SPEEK membranes with 0.2 wt.%, 0.5 wt.%, 1 wt.%, and 2 wt.% of CB[8].

CB[8]/SPEEK membranes. Notably, with the increase of CB[8] content, the C=O peak of CB[8] becomes progressively more pronounced (Fig. 2(b)). These findings confirm the incorporation of CB[*n*] molecules within the matrix of SPEEK.

3.3 Water uptake and swelling degree of CB[*n*]/SPEEK membranes

The proton conductivity of PEMs is strongly influenced by the presence of water [32, 33]. However, a high water content can lead to increased flexibility of the polymer chains, resulting in excessive swelling and compromising the dimensional stability of the membranes [14]. The water uptake and swelling degree of the pure SPEEK and CB[*n*]/SPEEK membranes are shown in Fig. 3. Notably, the addition of CB[*n*] to SPEEK membranes results in a decrease in water uptake at both 30 and 60 °C (Fig. 3(a)). Particularly, the water uptake of CB[8]/SPEEK-1% membrane (25.3%) is almost 5% less compared with that of pure SPEEK membrane (30.2%) at 60 °C. Moreover, the water uptake of CB[8]/SPEEK membranes shows dependence on the loading amount of CB[8] (Fig. 3(b)). As the loading amount of CB[8] increases from 0.2 wt.% to 2.0 wt.%, the water uptake of the membrane decreases from 28.7% to 24.1% at 60 °C. This decrease can be attributed to the less hydrophilic character of the CB[8], the rigid nature of CB[8], and the formation of hydrogen bonds between CB[8] and SPEEK [14, 44, 45]. The higher amount of CB[8] added results in a greater number of hydrogen bonds within the CB[8]/SPEEK membranes, leading to less motion of SPEEK chains [44, 45]. These observations align with the swelling degree results of the pure SPEEK and CB[*n*]/SPEEK membranes. The membranes containing 1 wt.% CB[*n*] show reduced swelling compared with the pure SPEEK membrane at both 30 and 60 °C (Fig. 3(c)). Among the CB[*n*]/SPEEK-1% membranes, CB[8]/SPEEK-1% exhibits the lowest swelling degree of 5.8% at 30 °C. Furthermore, Fig. 3(d) demonstrates a negative correlation between the swelling degree of CB[8]/SPEEK membranes and the added amount, decreasing from 14.8% for CB[8]/SPEEK-0.2% to 5.6% for CB[8]/SPEEK-2% at 60 °C. This behavior can be attributed to the hydrogen bonding interactions between CB[*n*] and SPEEK polymers, indicating improved mechanical stability and reduced swelling of the membranes.

3.4 IEC of SPEEK and CB[*n*]/SPEEK membranes

A sufficient IEC is crucial for establishing continuous proton-conducting pathways within the PEMs, thereby facilitating proton conduction [46]. Table 1 shows the IEC values of SPEEK and CB[*n*]/SPEEK membranes. It is evident from the table that the introduction of CB[*n*] into the SPEEK hybrid membranes results in a higher IEC compared with the pure SPEEK membrane. This

indicates that CB[*n*] contribute to the increase in the IEC, primarily due to its ability to conduct protons and introduce additional proton-conducting sites within the membranes. Notably, the CB[8]/SPEEK-1% membrane shows the highest IEC value of 1.94 mmol·g⁻¹. The IEC of CB[8]/SPEEK membranes shows an increasing trend with the added amount of CB[8] from 0.2 wt.% to 1 wt.%. However, the IEC of CB[8]/SPEEK-2% experiences a 3% decrease compared with CB[8]/SPEEK-1%. This reduction is likely due to the formation of small aggregations of CB[8] within the CB[8]/SPEEK-2% membrane, which hinders the release of protons by CB[8] [14].

3.5 Proton conductivity of the SPEEK and CB[*n*]/SPEEK membranes

Proton conductivity of PEMs plays a crucial role in the performance of PEMFCs [47]. In this study, inspired by the proton-conducting mechanism of transmembrane protein (bacteriorhodopsin) [24], CB[*n*] with similar proton-conducting mechanism, were introduced into the SPEEK matrix to enhance the proton conductivity. As shown in Fig. 4, ion–dipole interactions make the dipolar carbonyl-fringed portals of CB[*n*] highly appealing for proton binding, which can act as proton acceptors to bind and release protons [30]. In addition, the cavity can accommodate water molecules, contributing to the formation of hydrogen bond networks and providing additional proton pathways within the membrane [28–30]. Furthermore, the small molecular size (< 2 nm) and the organic molecular structure enable their dispersion in the SPEEK matrix without any defects [10, 34, 35]. The interface between CB[*n*] and the SPEEK matrix acts as a pathway, bridging the otherwise disconnected sulfonic acid ionic domains of SPEEK, and thereby enhancing the proton conductivity [36].

The proton conductivities of both the SPEEK and CB[*n*]/SPEEK membranes are shown in Fig. 5. All membranes exhibit a positive temperature–conductivity relationship, suggesting that the proton conduction within the membranes is a thermally activated process [48]. The proton conductivity is enhanced after the introduction of CB[*n*]. As shown in Fig. 5(a), the SPEEK membrane exhibits a proton conductivity of 33.8 mS·cm⁻¹ at 30 °C and 100% RH. In comparison, the proton conductivities of the CB[6]/SPEEK-1%, CB[7]/SPEEK-1%, and CB[8]/SPEEK-1% membranes are 70.1 mS·cm⁻¹ (107% increase), 37.0 mS·cm⁻¹ (10% increase), and 75.2 mS·cm⁻¹ (123% increase), respectively, under the same conditions. Notably, among these three CB[*n*] modified membranes CB[8]/SPEEK-1% shows the highest proton conductivity of 198.0 mS·cm⁻¹ at 60 °C, which is even comparable to that of Nafion 117 at 80 °C (122 mS·cm⁻¹)
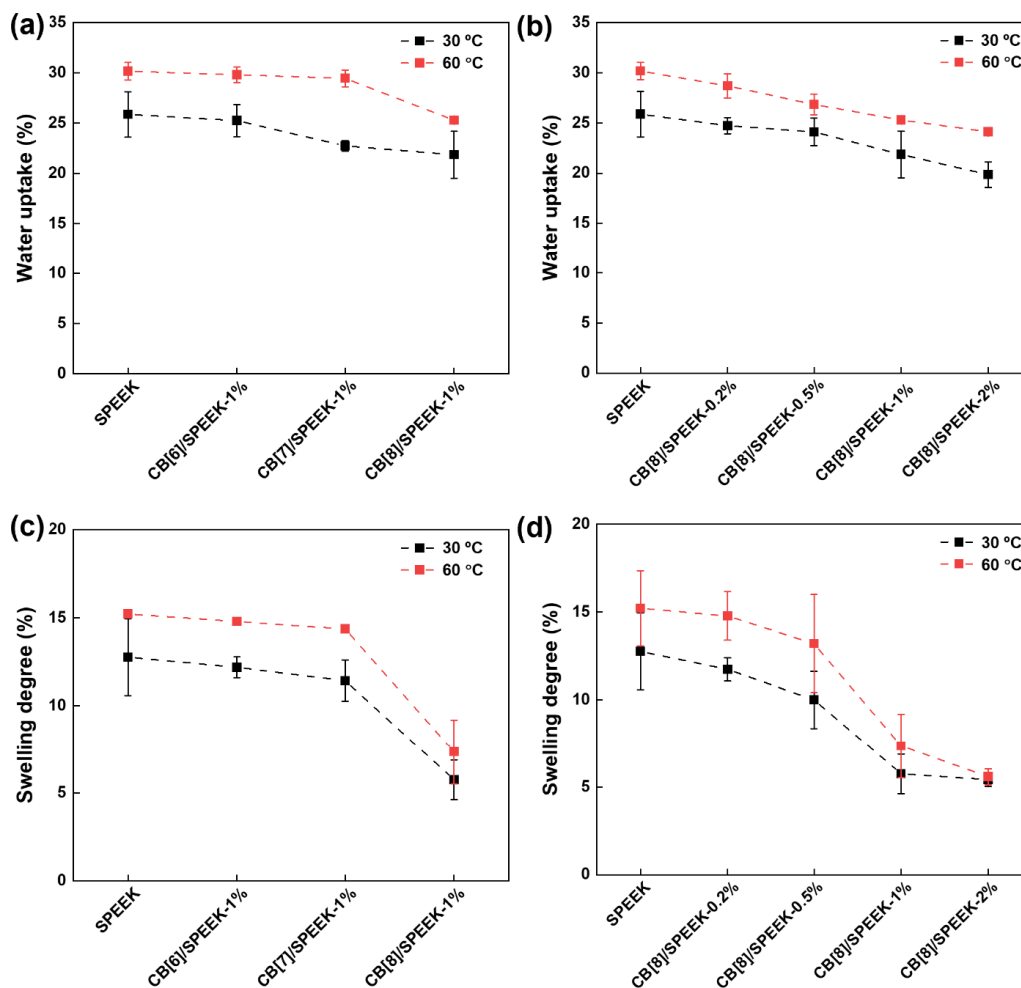
Figure 3 Water uptake of different membranes at 30 and 60 °C: (a) SPEEK with 1 wt.% CB[*n*], and (b) SPEEK with 0.2 wt.%, 0.5 wt.%, 1 wt.%, and 2 wt.% of CB[8]. Swelling degree of different membranes at 30 and 60 °C: (c) SPEEK with 1 wt.% CB[*n*], and (d) SPEEK with 0.2 wt.%, 0.5 wt.%, 1 wt.%, and 2 wt.% of CB[8].

**Table 1** The IEC values of SPEEK and CB[*n*]/SPEEK membranes

Entry	Membranes	IEC (mmol·g⁻¹)
1	SPEEK	1.80
2	CB[6]/SPEEK-1%	1.91
3	CB[7]/SPEEK-1%	1.84
4	CB[8]/SPEEK-1%	1.94
5	CB[8]/SPEEK-0.2%	1.85
6	CB[8]/SPEEK-0.5%	1.86
7	CB[8]/SPEEK-2%	1.88

[40]. As the CB[7] shows the highest residence time of water molecules and the highest energy barrier to cavity water molecules among the whole CB[*n*] family [30, 49], the proton conduction through CB[7] is slower than CB[6] and CB[8]. Consistently, the proton conductivity of the CB[7]/SPEEK-1% is lower than that of the CB[6]/SPEEK-1% membrane and CB[8]/SPEEK-1% membrane. Compared with CB[6], CB[8] contains a greater number of carbonyl groups, resulting in more proton-conducting sites. Moreover, CB[8] exhibits a larger cavity capable of accommodating more water molecules (13.1) than CB[6] (3.3), and it forms a greater number of hydrogen bonds between adjacent cavity water molecules (2.55) than CB[6] (1.31) [49]. Consequently, the proton conduction of the PEM with CB[8] offers more pathways than the PEM with CB[6] when the loading amount is the same.

CB[8] demonstrates more promising potential for developing

PEMs compared with CB[6] and CB[7]. Consequently, CB[8] was selected to investigate the effect of loading amount on proton conductivity. A series of hybrid membranes with different amounts of CB[8] (0 wt.%, 0.5 wt.%, 1 wt.%, and 2 wt.%) were prepared via the solution casting method. The proton conductivity of the CB[8]/SPEEK membranes was tested at different temperatures (Fig. 5(b)). With the increase in the amount of CB[8] loading from 0.2 wt.% to 1 wt.%, the proton conductivity of the hybrid membranes exhibits a continuous increase from 92.6 mS·cm⁻¹ to a maximum value of 198.0 mS·cm⁻¹ at 60 °C and 100% RH. However, when the CB[8] amount is further increased to 2 wt.%, the proton conductivity of the membrane decreases to 166.0 mS·cm⁻¹. This trend is consistent across different temperatures. The observed variation in proton conductivity can be attributed to the introduction of well-dispersed CB[8] molecules, which may form continuous hydrogen bond networks and bridge previously disconnected domains in the SPEEK membrane [36]. This enhancement in proton conductivity is a result of improved connectivity of proton pathways, which reaches its peak at a loading amount of 1 wt.% CB[8]. However, when the CB[8] content exceeds 1 wt.% and reaches 2 wt.%, small aggregates of CB[8] molecules may form. These aggregates obstruct the formation of efficient proton transport pathways and impede the release of protons from CB[8], thereby hindering proton conduction [50]. Therefore, careful optimization of the CB[8] loading in the hybrid membranes is crucial to achieving the highest conductivity.

The proton conductivity results of the membranes provide validation for the enhancement of proton conductivity by CB[*n*]. To investigate the proton conduction mechanism within the
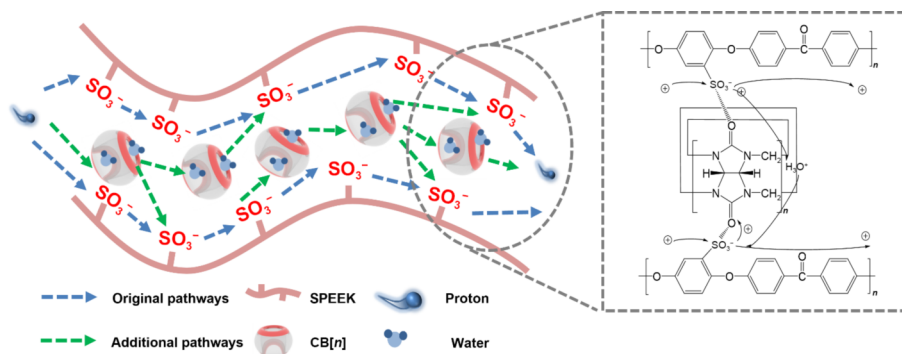
Figure 4 Schematic illustration of the proton conduction within the CB[*n*]/SPEEK membranes.
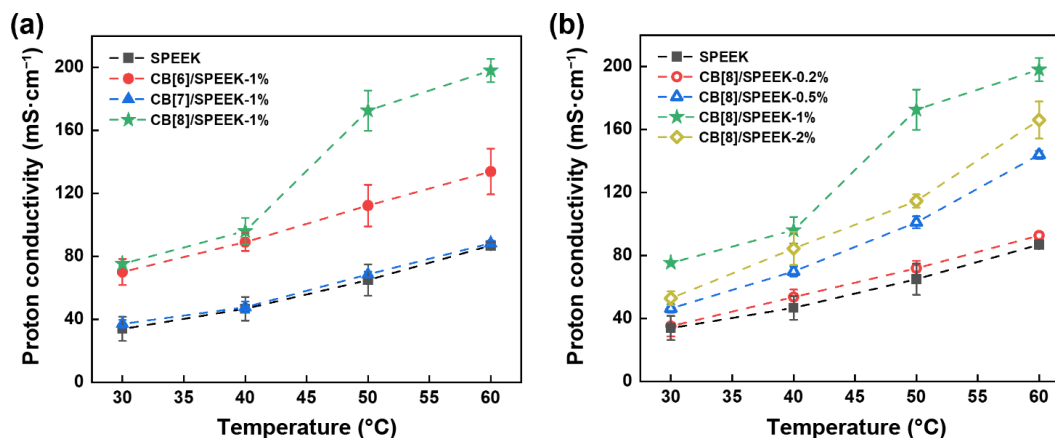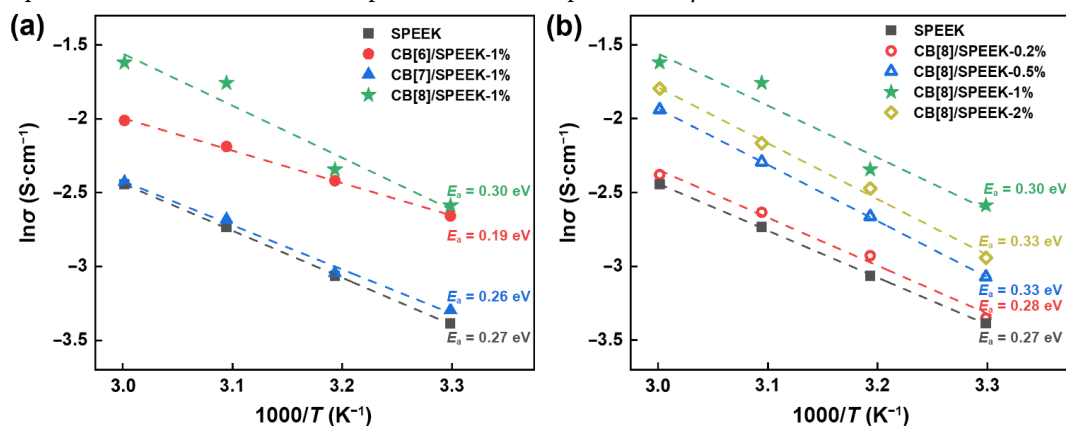

Figure 5 Proton conductivity for different membranes at 100% RH, as a function of temperature: (a) SPEEK with 1 wt.% CB[*n*] at 30 to 60 °C, and (b) SPEEK with 0.2 wt.%, 0.5 wt.%, 1 wt.%, and 2 wt.% of CB[8] at 30 to 60 °C.

membranes, activation energy of proton conduction in the membranes was calculated using the Arrhenius equation. As shown in Fig. 6(a), the E_a of proton conductivity in membranes containing 1 wt.% CB[*n*] is presented. The E_a value for the pure SPEEK membrane is determined to be 0.27 eV, which falls below the threshold of 0.4 eV. This indicates that proton conduction is primarily governed by the Grotthuss mechanism and supported by the vehicle mechanism [32]. The E_a values for the CB[6]/SPEEK-1%, CB[7]/SPEEK-1%, and CB[8]-SPEEK-1% membranes are 0.19, 0.26, and 0.30 eV, respectively. These values suggest that the proton-conducting mechanisms in the CB[*n*]/SPEEK membranes are consistent with those observed in the pure SPEEK membrane. Additionally, as depicted in Fig. 6(b), the E_a values of CB[8]/SPEEK membranes are all below 0.4 eV, indicating that they exhibit the same proton-conducting mechanisms as the pure SPEEK membrane.

3.6 Fuel cell performance

Polarization experiments were used to evaluate the performance of

the SPEEK and CB[*n*]/SPEEK membranes (Fig. 7). As shown in Fig. 7(a), CB[8]/SPEEK-1% outperforms other samples, with the highest power density of 214 mW·cm^{-2} when the current density reaches 424 mA·cm^{-2}. This represents a 140% improvement in peak power density (89 mW·cm^{-2}) over the SPEEK membrane obtained at 201 mA·cm^{-2}. With the addition of the same amount of CB[*n*], CB[8] and CB[6] lead to a more significantly enhanced PEMFC performance than CB[7], which is consistent with the proton conductivity results. To verify the result of the optimal CB[8] loading amount, the PEMFC performance of CB[8]/SPEEK membranes was tested as well (Fig. 7(b)). When the amount of CB[8] is 0.2 wt.%, the performance of the fuel cell is slightly improved compared with the pure SPEEK membrane. As the CB[8] addition increases to 0.5 wt.%, 1 wt.%, and 2 wt.%, it is apparent that the CB[8]/SPEEK membranes perform better than the pure SPEEK membrane, especially at higher current density (> 200 mA·cm^{-2}), where the performance reduces drastically. When the amount of CB[8] is 2 wt.%, the PEMFC exhibits a peak power density of 175 mW·cm^{-2} at 326 mA·cm^{-2}. This represents an

Figure 6 Arrhenius activation energy of proton conduction: (a) SPEEK with 1 wt.% of CB[*n*], and (b) SPEEK with 0.2 wt.%, 0.5 wt.%, 1 wt.%, and 2 wt.% of CB[8].
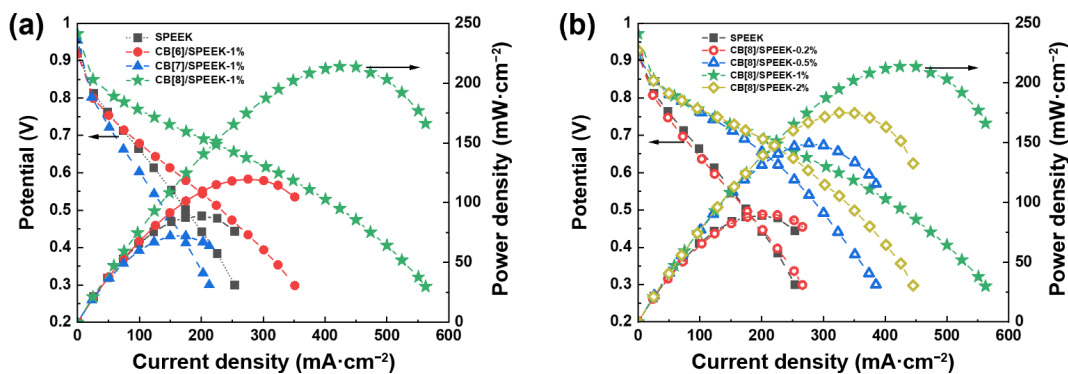
Figure 7 Polarization and power density curves for different membranes based PEMFCs at 50 °C cell temperature and 100% RH using hydrogen and air at stoichiometric ratios of 1.5 and 3, respectively: (a) SPEEK with 1 wt.% CB[*n*], and (b) SPEEK with 0.2 wt.%, 0.5 wt.%, 1 wt.%, and 2 wt.% of CB[8].

18% decrease in peak power density over the membrane with 1 wt.% CB[8]. This phenomenon can be attributed to an excessive amount of CB[8], which aggregates and blocks the construction of facile proton transport pathways, hindering proton conduction [50].

4   Conclusions

This work employed a systematic NICE methodology, which involved extracting biological mechanisms underpinning desired properties from bacteriorhodopsin to design and fabricate hybrid proton exchange membranes with enhanced properties. Drawing inspiration from the structure of bacteriorhodopsin, which features a hydrophobic cavity and hydrogen bond interactions, three types of supramolecular macrocycles (CB[*n*], *n* = 6, 7, or 8) with different amounts of repeating units were introduced into the SPEEK polymer matrix. The nanosize of the CB[*n*] molecules allows for their effective dispersion within the polymer matrix, avoiding dead zones or voids. The carbonyl groups of CB[*n*] facilitate the formation of hydrogen-bond networks with the sulfonic groups and water molecules within the membranes. This bridging effect enhances the continuity of proton transport pathways that may be less connected in the original SPEEK membrane, thereby promoting proton conduction. Among the membranes studied, the CB[8]-incorporated SPEEK membrane, with the highest number of carbonyl groups and hydrogen bonds, exhibits the most significant improvement in proton-conductivity compared with CB[6] and CB[7]. Furthermore, exploring different CB[8] loading amounts reveals that the introduction of CB[8] leads to increased proton conductivity, with the optimum loading amount determined to be 1 wt.%. This membrane demonstrates the highest proton conductivity of 198.0 mS·cm^{-1}, surpassing that of the pure SPEEK membrane by 114% at 60 °C and 100% RH, and even outperforming Nafion 117. Additionally, the CB[8]/SPEEK-1% achieves the highest power density of 214 mW·cm^{-2} at a current density of 424 mA·cm^{-2}, representing a substantial 140% improvement in peak power density (89 mW·cm^{-2}) compared with the pure SPEEK membrane obtained at 201 mA·cm^{-2}. These findings provide valuable insights into the investigation of supramolecular macrocycles for proton exchange membranes, highlighting their potential for enhancing fuel cell performance.

Acknowledgements

References

[1] Jacobson, M. Z.; Colella, W. G.; Golden, D. M. Cleaning the air and improving health with hydrogen fuel-cell vehicles. *Science.* **2005**, *308*, 1901–1905.

[2] Kreuer, K. D. Proton conductivity: Materials and applications. *Chem. Mater.* **1996**, *8*, 610–641.

[3] Kreuer, K. D.; Paddison, S. J.; Spohr, E.; Schuster, M. Transport in proton conductors for fuel-cell applications: Simulations, elementary reactions, and phenomenology. *Chem. Rev.* **2004**, *104*, 4637–4678.

[4] Laberty-Robert, C.; Vallé, K.; Pereira, F.; Sanchez, C. Design and properties of functional hybrid organic–inorganic membranes for fuel cells. *Chem. Soc. Rev.* **2011**, *40*, 961–1005.

[5] Hickner, M. A.; Ghassemi, H.; Kim, Y. S.; Einsla, B. R.; McGrath, J. E. Alternative polymer systems for proton exchange membranes (PEMs). *Chem. Rev.* **2004**, *104*, 4587–4612.

[6] Jiao, K.; Xuan, J.; Du, Q.; Bao, Z. M.; Xie, B.; Wang, B. W.; Zhao, Y.; Fan, L. H.; Wang, H. Z.; Hou, Z. J. et al. Designing the next generation of proton-exchange membrane fuel cells. *Nature* **2021**, *595*, 361–369.

[7] Park, C. H.; Kim, T. H.; Nam, S. Y.; Hong, Y. T. Water channel morphology of non-perfluorinated hydrocarbon proton exchange membrane under a low humidifying condition. *Int. J. Hydrogen Energy* **2019**, *44*, 2340–2348.

[8] Lyu, K. J.; Peng, Y. Q.; Xiao, L.; Lu, J. T.; Zhuang, L. Water induced phase segregation in hydrocarbon proton exchange membranes. *J. Energy Chem.* **2018**, *27*, 1517–1520.

[9] Escorihuela, J.; Narducci, R.; Compañ, V.; Costantino, F. Proton conductivity of composite polyelectrolyte membranes with metal-organic frameworks for fuel cell applications. *Adv. Mater. Interfaces* **2019**, *6*, 1801146.

[10] Zhao, G. D.; Zhao, H. J.; Zhuang, X. P.; Shi, L.; Cheng, B. W.; Xu, X. L.; Yin, Y. Nanofiber hybrid membranes: Progress and application in proton exchange membranes. *J. Mater. Chem. A* **2021**, *9*, 3729–3766.

[11] Zhang, Y. X.; Wang, H. X.; Qian, P. H.; Zhang, L.; Zhou, Y.; Shi, H. F. Hybrid proton exchange membrane of sulfonated poly(ether ether ketone) containing polydopamine-coated carbon nanotubes loaded phosphotungstic acid for vanadium redox flow battery. *J. Membr. Sci.* **2021**, *625*, 119159.

[12] Peng, Q.; Li, Y.; Qiu, M.; Shi, B. B.; He, X. Y.; Fan, C. Y.; Mao, X. L.; Wu, H.; Jiang, Z. Y. Enhancing proton conductivity of sulfonated poly(ether ether ketone)-based membranes by incorporating phosphotungstic-acid-coupled graphene oxide. *Ind. Eng. Chem. Res.* **2021**, *60*, 4460–4470.

[13] Bisht, S.; Balaguru, S.; Ramachandran, S. K.; Gangasalam, A.; Kweon, J. Proton exchange composite membranes comprising SiO$_2$, sulfonated SiO$_2$, and metal-organic frameworks loaded in SPEEK polymer for fuel cell applications. *J. Appl. Polym. Sci.* **2021**, *138*, 50530.

[14] Yin, Z. Y.; Geng, H. B.; Yang, P. F.; Shi, B. B.; Fan, C. Y.; Peng, Q.; Wu, H.; Jiang, Z. Y. Improved proton conduction of sulfonated poly(ether ether ketone) membrane by sulfonated covalent organic framework nanosheets. *Int. J. Hydrogen Energy* **2021**, *46*, 26550–26559.

[15] Li, P.; Dang, J. C.; Wu, W. J.; Lin, J. L.; Zhou, Z. F.; Zhang, J.; Wang, J. T. Nanofiber composite membrane using quantum dot hybridized SPEEK nanofiber for efficient through-plane proton conduction. *J. Membr. Sci.* **2020**, *609*, 118198.

[16] Simari, C.; Enotiadis, A.; Lo Vecchio, C.; Baglio, V.; Coppola, L.; Nicotera, I. Advances in hybrid composite membranes engineering for high-performance direct methanol fuel cells by alignment of 2D nanostructures and a dual-layer approach. *J. Membr. Sci.* **2020**, *599*, 117858.

[17] Hou, C. L.; Zhang, X.; Li, Y. F.; Zhou, G. L.; Wang, J. T. Porous nanofibrous composite membrane for unparalleled proton conduction. *J. Membr. Sci.* **2018**, *550*, 136–144.

[18] Prykhodko, Y.; Fatyeyeva, K.; Hespel, L.; Marais, S. Progress in hybrid composite Nafion®-based membranes for proton exchange fuel cell application. *Chem. Eng. J.* **2021**, *409*, 127329.

[19] Lee, H.; Han, J.; Kim, K.; Kim, J.; Kim, E.; Shin, H.; Lee, J. C. Highly sulfonated polymer-grafted graphene oxide composite membranes for proton exchange membrane fuel cells. *J. Ind. Eng. Chem.* **2019**, *74*, 223–232.

[20] Esmaeili, N.; Gray, E. M.; Webb, C. J. Non-fluorinated polymer composite proton exchange membranes for fuel cell applications—A review. *ChemPhysChem* **2019**, *20*, 2016–2053.

[21] Wang, L. Y.; Deng, N. P.; Wang, G.; Ju, J. G.; Cheng, B. W.; Kang, W. M. Constructing amino-functionalized flower-like metal-organic framework nanofibers in sulfonated poly(ether sulfone) proton exchange membrane for simultaneously enhancing interface compatibility and proton conduction. *ACS Appl. Mater. Interfaces* **2019**, *11*, 39979–39990.

[22] Wang, S. J.; Zhu, T. H.; Shi, B. B.; Fan, C. Y.; Liu, Y. Q.; Yin, Z. Y.; Gao, Z.; Zhang, Z. J.; Wu, H.; Jiang, Z. Y. Porous organic polymer with high-density phosphoric acid groups as filler for hybrid proton exchange membranes. *J. Membr. Sci.* **2023**, *666*, 121147.

[23] Subramaniam, S.; Henderson, R. Molecular mechanism of vectorial proton translocation by bacteriorhodopsin. *Nature* **2000**, *406*, 653–657.

[24] Nango, E.; Royant, A.; Kubo, M.; Nakane, T.; Wickstrand, C.; Kimura, T.; Tanaka, T.; Tono, K.; Song, C. Y.; Tanaka, R. et al. A three-dimensional movie of structural changes in bacteriorhodopsin. *Science*. **2016**, *354*, 1552–1557.

[25] Trogadas, P.; Cho, J. I. S.; Neville, T. P.; Marquis, J.; Wu, B.; Brett, D. J. L.; Coppens, M. O. A lung-inspired approach to scalable and robust fuel cell design. *Energy Environ. Sci.* **2018**, *11*, 136–143.

[26] Coppens, M. O. Nature-inspired chemical engineering for process intensification. *Annu. Rev. Chem. Biomol. Eng.* **2021**, *12*, 187–215.

[27] Trogadas, P.; Coppens, M. O. Nature-inspired electrocatalysts and devices for energy conversion. *Chem. Soc. Rev.* **2020**, *49*, 3107–3141.

[28] Yoon, M.; Suh, K.; Kim, H.; Kim, Y.; Selvapalam, N.; Kim, K. High and highly anisotropic proton conductivity in organic molecular porous materials. *Angew. Chem., Int. Ed.* **2011**, *50*, 7870–7873.

[29] Liang, Y.; Li, E.; Wang, K. Y.; Guan, Z. J.; He, H. H.; Zhang, L. L.; Zhou, H. C.; Huang, F. H.; Fang, Y. Organo-macrocycle-containing hierarchical metal-organic frameworks and cages: Design, structures, and applications. *Chem. Soc. Rev.* **2022**, *51*, 8378–8405.

[30] Barrow, S. J.; Kasera, S.; Rowland, M. J.; Del Barrio, J.; Scherman, O. A. Cucurbituril-based molecular recognition. *Chem. Rev.* **2015**, *115*, 12320–12406.

[31] Chio, W. I. K.; Xie, H. M.; Zhang, Y. W.; Lan, Y.; Lee, T. C. SERS biosensors based on cucurbituril-mediated nanoaggregates for wastewater-based epidemiology. *TrAC Trends Analyt. Chem.* **2022**, *146*, 116485.

[32] Cukierman, S. Et tu, Grotthuss! And other unfinished stories. *Biochim. Biophys. Acta Bioenerg.* **2006**, *1757*, 876–885.

[33] Kreuer, K. D.; Rabenau, A.; Weppner, W. Vehicle mechanism, a new model for the interpretation of the conductivity of fast proton conductors. *Angew. Chem., Int. Ed.* **1982**, *21*, 208–209.

[34] Cheng, Y. D.; Ying, Y. P.; Japip, S.; Jiang, S. D.; Chung, T. S.; Zhang, S.; Zhao, D. Advanced porous materials in mixed matrix membranes. *Adv. Mater.* **2018**, *30*, 1802401.

[35] Feng, L.; Hou, H. B.; Zhou, H. UiO-66 derivatives and their composite membranes for effective proton conduction. *Dalton Trans.* **2020**, *49*, 17130–17139.

[36] He, G. W.; Nie, L. L.; Han, X.; Dong, H.; Li, Y. F.; Wu, H.; He, X. Y.; Hu, J. B.; Jiang, Z. Y. Constructing facile proton-conduction pathway within sulfonated poly(ether ether ketone) membrane by incorporating poly(phosphonic acid)/silica nanotubes. *J. Power Sources.* **2014**, *259*, 203–212.

[37] Kim, J.; Jung, I. S.; Kim, S. Y.; Lee, E.; Kang, J. K.; Sakamoto, S.; Yamaguchi, K.; Kim, K. New cucurbituril homologues: Syntheses, isolation, characterization, and X-ray crystal structures of cucurbit[*n*]uril (*n* = 5, 7, and 8). *J. Am. Chem. Soc.* **2000**, *122*, 540–541.

[38] Jansen, K.; Buschmann, H. J.; Wego, A.; Döpp, D.; Mayer, C.; Drexler, H. J.; Holdt, H. J.; Schollmeyer, E. Cucurbit[5]uril, decamethylcucurbit[5]uril, and cucurbit[6]uril. Synthesis, solubility, and amine complex formation. *J. Incl. Phenom. Macrocycl. Chem.* **2001**, *39*, 357–363.

[39] Yang, P. F.; Wu, H.; Khan, N. A.; Shi, B. B.; He, X. Y.; Cao, L.; Mao, X. L.; Zhao, R.; Qiu, M.; Jiang, Z. Y. Intrinsic proton conductive deoxyribonucleic acid (DNA) intercalated graphene oxide membrane for high-efficiency proton conduction. *J. Membr. Sci.* **2020**, *606*, 118136.

[40] Zhang, P. P.; Li, W.; Wang, L.; Gong, C. L.; Ding, J. H.; Huang, C. S.; Zhang, X. D.; Zhang, S. J.; Wang, L.; Bu, W. F. Polydopamine-modified sulfonated polyhedral oligomeric silsesquioxane: An appealing nanofiller to address the trade-off between conductivity and stabilities for proton exchange membrane. *J. Membr. Sci.* **2020**, *596*, 117734.

[41] Guan, Z. F.; Jin, Y. Q.; Shi, S.; Jin, B. Y.; Zhang, M. S.; Zhao, L. H. Self-assembled proton conduction networks consisting of SPEEK, NH₂-POSS, and IL with enhanced proton conduction and decreased IL loss. *Polymer* **2022**, *254*, 125011.

[42] Wu, J.; Nie, S. J.; Liu, H.; Gong, C. L.; Zhang, Q. Y.; Xu, Z. S.; Liao, G. F. Design and development of nucleobase modified sulfonated poly(ether ether ketone) membranes for high-performance direct methanol fuel cells. *J. Mater. Chem. A* **2022**, *10*, 19914–19924.

[43] Tang, M. J.; Liu, M. L.; Wang, D. A.; Shao, D. D.; Wang, H. J.; Cui, Z. L.; Cao, X. L.; Sun, S. P. Precisely patterned nanostrand surface of cucurbituril[*n*]-based nanofiltration membranes for effective alcohol–water condensation. *Nano Lett.* **2020**, *20*, 2717–2723.

[44] Cao, L.; Shen, X. H.; Yang, X.; Zhang, B.; Li, Z. Y.; Gang, M. Y.; Wang, C. B.; Wu, H.; Jiang, Z. Y. Enhanced proton conductivity of proton exchange membranes by incorporating phosphorylated hollow titania spheres. *RSC Adv.* **2016**, *6*, 68407–68415.

[45] Singha, S.; Jana, T. Structure and properties of polybenzimidazole/silica nanocomposite electrolyte membrane: Influence of organic/inorganic interface. *ACS Appl. Mater. Interfaces* **2014**, *6*, 21286–21296.

[46] Cao, L.; He, X. Y.; Jiang, Z. Y.; Li, X. Q.; Li, Y. F.; Ren, Y. X.; Yang, L. X.; Wu, H. Channel-facilitated molecule and ion transport across polymer composite membranes. *Chem. Soc. Rev.* **2017**, *46*, 6725–6745.

[47] Alashkar, A.; Al-Othman, A.; Tawalbeh, M.; Qasim, M. A critical review on the use of ionic liquids in proton exchange membrane fuel cells. *Membranes* **2022**, *12*, 178.

[48] Mondal, S.; Agam, Y.; Nandi, R.; Amdursky, N. Exploring long-range proton conduction, the conduction mechanism and inner hydration state of protein biopolymers. *Chem. Sci.* **2020**, *11*, 3547–3556.

[49] Biedermann, F.; Uzunova, V. D.; Scherman, O. A.; Nau, W. M.; De Simone, A. Release of high-energy water as an essential driving force for the high-affinity binding of cucurbit[*n*]urils. *J. Am. Chem. Soc.* **2012**, *134*, 15318–15323.

[50] Xue, Q.; Yang, D. J.; Wang, J.; Li, B.; Ming, P. W.; Zhang, C. M. Enhanced mass transfer and proton conduction of cathode catalyst layer for proton exchange membrane fuel cell through filling polyhedral oligomeric silsesquioxane. *J. Power Sources* **2021**, *487*, 229413.